GaitGS: Temporal Feature Learning in Granularity and Span Dimension for Gait Recognition

Haijun Xiong[1]*
xionghj@hust.edu.cn

Yunze Deng[2]*
k2so4@ccnu.edu.cn

Xiaohu Huang[1]
huangxiaohu@hust.edu.cn

Xinggang Wang[1]
xgwang@hust.edu.cn

Wenyu Liu[1]
liuwy@hust.edu.cn

Bin Feng[1]†
fengbin@hust.edu.cn

[1]Huazhong University of Science and Technology
[2]Central China Normal University

Abstract

Gait recognition is an emerging biological recognition technology that identifies and verifies individuals based on their walking patterns. However, many current methods are limited in their use of temporal information. In order to fully harness the potential of gait recognition, it is crucial to consider temporal features at various granularities and spans. Hence, in this paper, we propose a novel framework named *GaitGS*, which aggregates temporal features in the *granularity* dimension and *span* dimension simultaneously. Specifically, Multi-Granularity Feature Extractor (MGFE) is proposed to focus on capturing the micro-motion and macro-motion information at the frame level and unit level respectively. Moreover, we present Multi-Span Feature Learning (MSFL) module to generate global and local temporal representations. On three popular gait datasets, extensive experiments demonstrate the state-of-the-art performance of our method. Our method achieves the Rank-1 accuracies of 92.9% (+0.5%), 52.0% (+1.4%), and 97.5% (+0.8%) on CASIA-B, GREW, and OU-MVLP respectively. The source code will be released soon.

1 Introduction

Gait recognition is a biometric technology that can identify humans through their distinct walking patterns [2]. Compared to other biometrics, such as faces, irises, fingerprints, and veins, gait is difficult to disguise and has no requirement for the cooperation of subjects during recognition [26, 24, 22, 3]. Thus, gait recognition has been widely applied in intelligent security systems, video surveillance, sport science, and crime prevention [25]. However, the performance of gait recognition is hindered by some realistic variations, *e.g.*, walking speed and clothing changes [5]. As a result, improving gait recognition technology and its ability to handle these challenges remains an ongoing area of innovation and development.

Currently, most gait recognition approaches [10, 19, 20, 14, 13, 36, 37, 32, 7, 37] consider it is crucial to capture temporal clues. Fan *et al.* [10] proposed a micro-motion capture module (MCM), which extracts temporal features at the frame level. Wang *et al.* [32] divided gait period into several phases, each of which was fused into a single image with temporal information to produce a Chrono-Gait Image (CGI). Lin *et al.* [20] proposed a Local Temporal Aggregation (LTA) operation to obtain

---

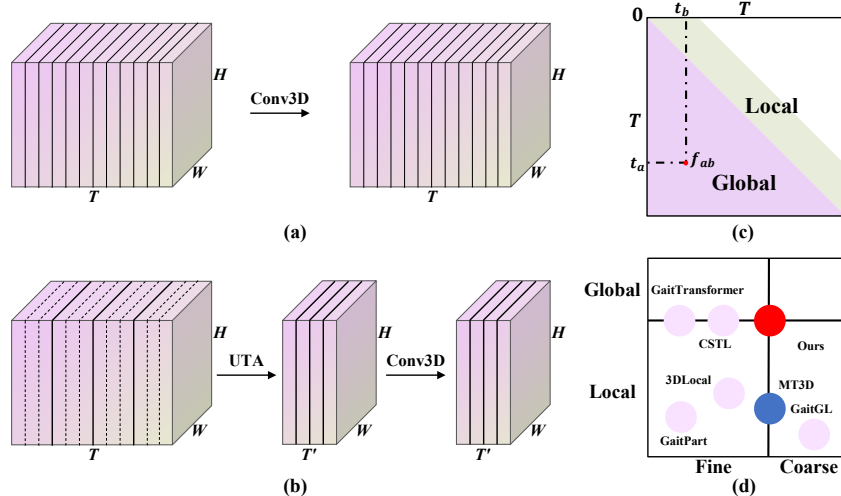*Contribute equally

†Corresponding author

Figure 1: (a) Fine-level temporal feature extraction. (b) Coarse-level temporal feature extraction. The input sequence is first processed by the Unit Temporal Aggregation (UTA) block to extract coarse-level features. (c) Global and Local temporal feature extraction. Mauve and light green represent global and local temporal feature learning, respectively. The red point indicates the relationship representation f_{ab} between the frame t_a and t_b. (d) Comparison of temporal modeling approaches in previous gait recognition models. For example, the blue circle indicates that MT3D [19] considers local temporal information at both fine and coarse levels, while the red circle shows that our method comprehensively models temporal information from four aspects.

local-range temporal information. Cui *et al.* [7] and Li *et al.* [17] designed transformers for global gait temporal modeling. Zhang *et al.* [37] utilized several parrel LSTMs to learn long-short term feature representations of different body parts. Huang *et al.* [13] proposed a temporal modeling network CSTL to aggregate frame-level, short-term and long-term temporal features. From these methods, we believe that rich discriminative temporal features are embedded in time series of various granularities and spans. Here *granularity* refers to the level of detail at which the gait features are learned, while *span* refers to the length of time over which these features are analyzed.

From the above analysis, temporal feature learning methods for the granularity dimension can be grouped into fine-level representation and coarse-level representation. Likewise, for the span dimension, these methods can be divided into two categories: global temporal representation and local temporal representation. For example, as shown in Figure 1 (d), MT3D [19] considers the local temporal clues in individual frames, while GaitGL [20] exclusively focuses on coarse-level local temporal information. However, current methods model temporal information either from the granularity dimension or the span dimension, which hinders recognition performance significantly.

To tackle this issue, we propose a novel framework named ***GaitGS*** for gait recognition which models temporal features from both the granularity dimension and span dimension simultaneously. Specifically, we introduce a Multi-Granularity Feature Extractor (MGFE), which consists of two branches: the fine branch and the coarse branch. The fine branch takes the original sequence (Figure 1 (a)) as input, while the coarse branch takes the aggregation sequence (Figure 1 (b)) as input and continually incorporates features from the fine branch. Additionally, we propose a Multi-Span Feature Learning (MSFL) module for global and local temporal modeling at both the fine branch and coarse branch simultaneously, which consists of a transformer [30] block and MCM [10].

However, traditional position encoding [30, 8] seriously harms the flexibility of transformers. For instance, the fixed length of the learnable positional encoding makes it difficult to handle longer sequences than the training data during testing, while the sinusoidal positional encoding is hard to focus on the variability of different sequences. To address this, we utilize group convolution to extract the temporal position relationships in an adaptive manner. By combining both these aspects, we can obtain more discriminative temporal representations, which improves the performance of gait recognition.

The main contributions of our work can be summarized as follows:

- In this paper, we propose a novel effective framework GaitGS for gait recognition, which models temporal information from both the granularity dimension and span dimension simultaneously.

- We propose a Multi-Granularity Feature Extractor (MGFE), which comprises both a fine branch and a coarse branch. The fine branch focuses on capturing the micro-motion clues, while the coarse branch focuses on the macro-motion clues.

- Additionally, we introduce a Multi-Span Feature Learning (MSFL) module to extract comprehensive global and local temporal representations. To address the limitations of traditional position encoding, we utilize group convolution to generate temporal position information adaptively.

- Extensive experiments on three public datasets, CASIA-B [34], GREW [38], and OU-MVLP [27] demonstrate the state-of-the-art performance of. Furthermore, ablation experiments confirm the effectiveness of our proposed modules.

2 Related Work

Gait Recognition. Current gait recognition methods can be broadly classified into model-based and appearance-based categories. **Model-based** methods [16, 18, 29, 28, 35, 23, 1, 31] analyze the human structure to extract body models, such as 2D and 3D pose, which are regarded as network inputs to extract the subject identity features. For example, Teepe *et al.* [29, 28] generated gait features by Graph Convolutional Networks (GCN) for 2D pose modeling. Zhang *et al.* [35] and Pinyoanuntapong *et al.* [23] extract the spatial information of keypoints via self-attention mechanism. **Appearance-based** methods [11, 36, 37, 4, 10, 19, 20, 14, 13, 7, 33, 6] learn gait features directly from the human morphology of the input sequence and can perform recognition tasks at low resolution. Han *et al.* [11] synthesized the gait sequence as a Gait Energy Image (GEI) after normalizing the body region and the image centre of gravity. Huang *et al.* [13] and Lin *et al.* [20] extracted the spatial-temporal features by CNN. Compared to model-based methods, the features extracted from appearance-based methods contain richer spatial-temporal information.

Temporal Modeling. Chao *et al.* [4] regarded the gait sequence as an unordered set, which neglects temporal information. As shown in Figure 1 (d), most gait recognition methods [37, 10, 19, 20, 14, 13, 7] model temporal information either in the granularity dimension or span dimension. Zhang *et al.* [37] proposed an Auto-Encoder framework to learn long-short temporal feature representations in a three-layer LSTM. Fan *et al.* [10] focused on exploring local-range micro-motion information of corresponding parts through parallel MCMs. Lin *et al.* [20] used 3D CNNs to learn coarse-level temporal feature representations. Huang *et al.* [13] designed a Context-Sensitive Temporal Feature Learning (CSTL) network to aggregate frame-level, short-term, and long-term temporal features in an adaptive manner. Cui *et al.* [7] proposed the Multiple-Temporal-Scale Transformer (MTST) module for global-range temporal modeling.

However, the above approaches model temporal information either from the granularity dimension or from the span dimension, which hinders recognition performance significantly. Therefore, in this paper, we propose an effective framework GaitGS, which models temporal information from both the granularity dimension and span dimension simultaneously. We propose MGFE to capture the micro-motion and macro-motion information at the granularity dimension. Additionally, we design MSFL module for learning the global and local temporal representations at the span dimension. By aggregating these four different types of temporal features, the proposed GaitGS generates more robust gait representations.

3 Method

In this section, we provide an overview of the GaitGS pipeline and elaborate on the modules of the network in detail, including Multi-Granularity Feature Extractor (MGFE) and Multi-Span Feature Learning (MSFL). We also introduce the details of the loss functions used in our approach.
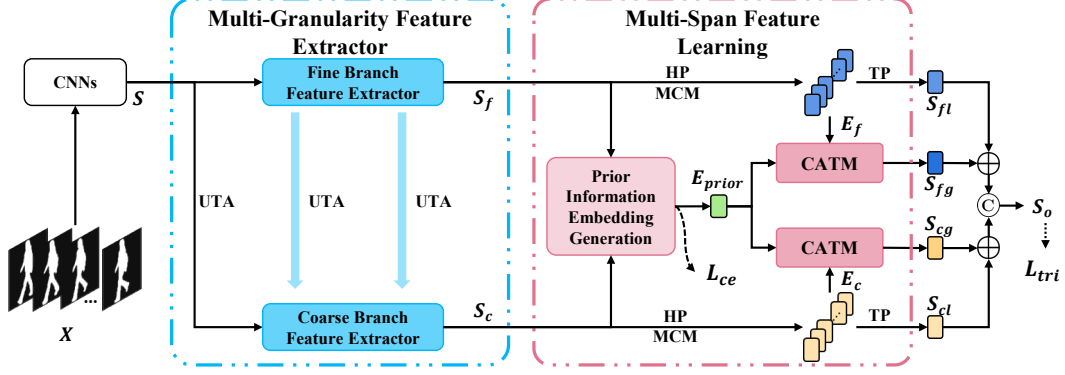
Figure 2: Overview of GaitGS. The target of UTA operation is to aggregate the fine-level feature. MGFE extracts the fine-level feature S_f and coarse-level feature S_c from the shallow feature S. MSFL produces four types of temporal features, which are the local fine-level temporal feature S_{fl}, global fine-level temporal feature S_{fg}, local coarse-level temporal feature S_{cl}, and global coarse-level temporal feature S_{cg} respectively. Finally, the recombined feature S_o is obtained by aggregating S_{fl}, S_{fg}, S_{cl} and S_{cg}. HP stands for Horizontal Pooling, MCM [10] represents the micro-motion capture module, and TP stands for Temporal Pooling. L_{tri} and L_{ce} represent triplet loss and cross-entropy loss respectively.

3.1 Network Pipeline

As shown in Figure 2, we propose a novel gait recognition framework called GaitGS, which consists of two major components: MGFE and MSFL. Assuming that the input gait sequence X is defined as size $1 \times T \times H \times W$, where T, H and W represent the length, height and width of the sequence, respectively. First, a set of 3D CNNs extracts the shallow spatial-temporal feature S. Then, MGFE extracts the fine- and coarse-level features S_f and S_c simultaneously. To enhance the representation ability of S_c, the fine-level feature S_f is added to the coarse-level feature S_c through the Unit Temporal Aggregation (UTA) operation. Next, we propose the MSFL module to obtain global and local temporal feature representations S_{fl}, S_{fg}, S_{cl} and S_{cg} by using Channel-Adaptive Transformer Module (CATM) and MCM [10] at the fine branch and coarse branch, respectively. Finally, a more robust feature representation S_o is obtained by aggregating four types of temporal features extracted from MSFL. The entire network is trained by using both triplet loss and cross-entropy loss.

3.2 Multi-Granularity Feature Extractor

As shown in Figure 2, we propose an effective dual-branch feature extractor named MGFE to model temporal information of the diverse granularity. Its core component is Spatial-Temporal Enhanced Module (STEM) based on B3D [19].

Spatial-Temporal Enhanced Module. As shown in Figure 3 (a), the input feature $X_s \in \mathbb{R}^{c \times t \times h \times w}$ is first split into four parts in the height dimension, denoted as $X_{hp} = \{X_{hp}^i | i = 1, 2, 3, 4\}$. Then, the plain network of STEM extracts feature representations with four B3Ds, which share the convolutional weights. Additionally, the shortcut branch uses a B3D to enhance feature representations. The output of the STEM layer can be denoted as:

$$X_{STEM} = \text{Cat}\{\text{B3D}(X_{hp}^i)\} + \text{B3D}(X_s), i = 1, 2, 3, 4. \tag{1}$$

Each B3D uses parallel convolutions with kernel size $(3, 3, 3)$, $(3, 1, 1)$ and $(1, 3, 3)$ to extract spatial-temporal feature, pixel-level motion feature and salient spatial feature respectively. Afterwards, these three kinds of features are fused into the final enhanced features by adding them together.

Feature Extractor. As shown in Figure 3 (b), we construct the Fine Branch and Coarse Branch Feature Extractor based on STEM to generate temporal feature representations of different granularities. The Fine Branch Feature Extractor consists of several STEMs and MaxPooling, which can be denoted as:

$$S_f = \text{G}(\text{G}(\text{MaxPool}^{1 \times 2 \times 2}(\text{G}(\hat{S}_f)))), \tag{2}$$
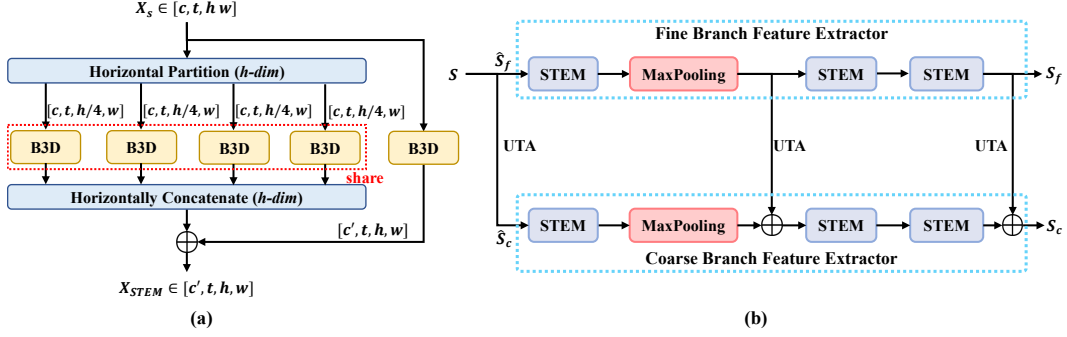
4

Figure 3: (a) The structure of STEM. B3D [19] consists of three 3D CNNs with kernel size $(3, 3, 3)$, $(3, 1, 1)$ and $(1, 3, 3)$, respectively. (b) Details of MGFE, which consists of a Fine Branch Feature Extractor and a Coarse Branch Feature Extractor.

where $\hat{S}_f \in \mathbb{R}^{C_1 \times T \times H \times W}$ and $S_f \in \mathbb{R}^{C_2 \times T \times H_2 \times W_2}$ are the input and output of Fine Branch Feature Extractor, and $G(\cdot)$ denotes STEM module. For the Coarse Branch Feature Extractor, the input feature $\hat{S}_c$ is produced from $\hat{S}_f$ by UTA operation, which can be denoted as:

$$\hat{S}_c = \sigma(\text{Conv}_{3\times1\times1}^{3\times1\times1}(\hat{S}_f)), \tag{3}$$

where $\hat{S}_c \in \mathbb{R}^{C_1 \times T' \times H \times W}$, $\text{Conv}_{3\times1\times1}^{3\times1\times1}(\cdot)$ is a 3D convolution with kernel size $(3, 1, 1)$ and stride $(3, 1, 1)$, and σ denotes the activation function. The coarse-level feature $S_c \in \mathbb{R}^{C_2 \times T' \times H_2 \times W_2}$ is obtained in a similar way to the fine branch. Additionally, we use UTA operation to enrich the representation of the coarse-level feature by constantly adding fine-level information.

3.3 Multi-Span Feature Learning

In order to comprehensively mine global and local temporal clues, we propose the MSFL module, which consists of two major parts, *i.e.*, Prior Information Embedding Generation (PIEG) and Channel-Adaptive Transformer Module (CATM).

Prior Information Embedding Generation. Fine- and coarse-level features S_f, S_c are still susceptible to changes in non-visual factors, such as camera view and carrying condition. Therefore, we introduce PIEG to acquire prior information embedding E_{prior} to reduce the interference of gait-unrelated features and enhance the robustness of the gait representation. As shown in Figure 4, we first aggregate the fine- and coarse-level features S_f and S_c, which can be represented as:

$$S_{prior} = \left(\text{SP}\left((\text{Cat}\left\{\text{TP}(S_f), \text{TP}(S_c)\right\})^p\right)\right)^{1/p}, \tag{4}$$

where TP and SP denote temporal and spatial pooling respectively, and p is a learnable parameter. Then, we select the embedding E_{prior} by the maximum probability $\hat{y}$, which can be formulated as:

$$\hat{y} = \arg\max\hat{p} \quad \text{and} \quad \hat{p} = W_{prior} \times S_{prior}, \tag{5}$$

where $\hat{y} \in \{0, 1, \cdots, M-1\}$, $W_{prior} \in \mathbb{R}^{M \times 2C_2}$ is the weight matrix. M is the number of a type of prior information, for example, in CASIA-B [34], $M = 3$ for conditions and $M = 11$ for views. To obtain accurate E_{prior}, we use cross-entropy loss L_{ce} to supervise $\hat{p}$ generated by Equation (5).
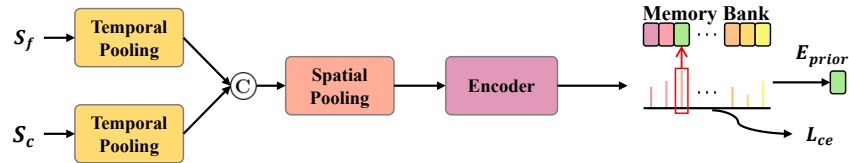

Figure 4: Structure of PIEG Module. The maximum score is indicated by the red box, while the selected embedding is highlighted by the red arrow.

Channel-Adaptive Transformer Module. We design a transformer-based module CATM to mine global temporal information. As shown in Figure 5, taking the generation process of the global
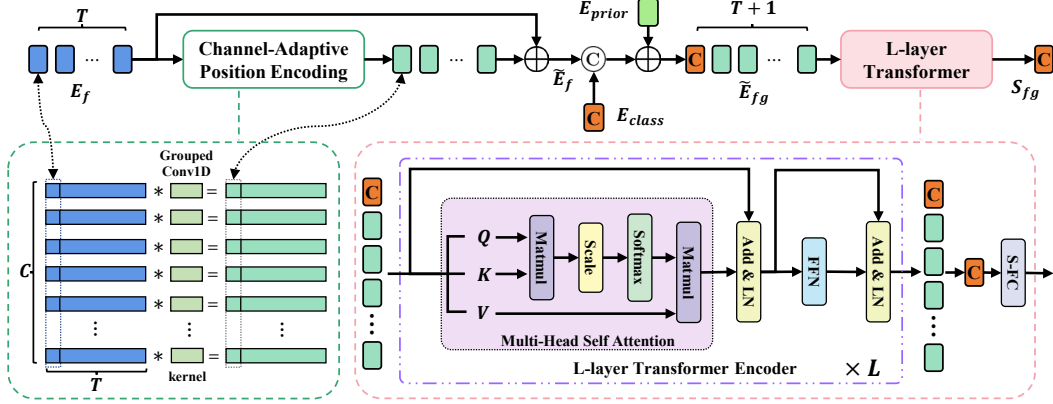
Figure 5: Details of CATM. Taking the generation process of fine-level global temporal feature S_{fg} as an example.

fine-level feature S_{fg} as an example. CATM takes prior information embedding E_{prior} and feature embedding E_f as inputs. The fine-level feature embedding can be represented as:

$$E_f = \text{MCM}(\text{HP}(S_f)), \tag{6}$$

where $\text{MCM}(\cdot)$ and $\text{HP}(\cdot)$ denotes Micro-motion Capture Module and Horizontal Pooling operation respectively. Then we introduce a grouped 1D CNN with kernel size K, which adaptively aggregates adjacent frames to extract implicit position information for each channel. This operation ensures the order of gait frames and is suitable for any frame-length sequence during the test phase. Feature embedding after position embedding can be written as:

$$\tilde{E}_f = E_f + \text{GConv}^K(E_f) = \{\tilde{E}_f^i | i = 1, 2, ..., T\}, \tag{7}$$

where $\text{GConv}^K(\cdot)$ denotes a grouped 1D CNN with kernel size K. Moreover, we introduce a learnable class token embedding E_{class} for aggregating temporal information and the prior information embedding E_{prior}, which can be denoted as:

$$\tilde{E}_{fg} = \text{Cat}\{\tilde{E}_f, E_{class}\} + E_{prior}. \tag{8}$$

Afterwards, a transformer encoder with L layers and N-head self-attention blocks extracts global temporal features. Subsequently, the class token is taken and passed through a Separate FC layer to obtain the final global fine-level feature S_{fg}, denoted as:

$$S_{fg} = \text{SFc}(\text{LTE}(\tilde{E}_{fg})[class]), \tag{9}$$

where $\text{LTE}(\cdot)$ and $\text{SFc}(\cdot)$ represent L-Transformer Encoder and Separate FC operation respectively.

In addition, the local fine-level feature can be obtained by:

$$S_{fl} = \text{TP}(E_f). \tag{10}$$

In the same way, we can obtain the global coarse-level feature S_{cg} and local coarse-level feature S_{cl}. Finally, we fuse gait features at different granularities and spans to obtain a robust and discriminative gait representation, which can be formulated as:

$$S_o = \text{Cat}\{S_{fg} + S_{fl}, S_{cg} + S_{cl}\}. \tag{11}$$

3.4 Loss function

To efficiently train the proposed network, we introduce both triplet loss L_{tri} and cross-entropy loss L_{ce}. The former aims to increase inter-class distance and reduce intra-class distance, while the latter aims to improve the accuracy of prior information embedding. The final loss can be represented as:

$$L = L_{tri} + \alpha L_{ce}, \tag{12}$$

with

$$L_{tri} = \max\left(d(x_a, x_p) - d(x_a, x_n) + m, 0\right), \tag{13}$$

where α is the weight of cross-entropy. x_a and x_p are samples from the same subjects, while x_a and x_s are from different subjects. $d(\cdot)$ denotes the Euclidean distance and m is the margin of the triplet loss.

Table 1: Rank-1 accuracy (%) on CASIA-B under all view angles with different conditions, excluding identical-view case. Bold and underline represent the best and second best, respectively. * denotes the method is trained with the data augmentation strategy.

Gallery NM		0°-180°										Mean
	Probe	0°	18°	36°	54°	72°	90°	108°	126°	144°	162°	180°	
NM	GaitSet [4]	91.1	99.0	**99.9**	97.8	95.1	94.5	96.1	98.3	99.2	98.1	88.0	96.1
	GaitPart [10]	94.1	98.6	99.3	98.5	94.0	92.3	95.9	98.4	99.2	97.8	90.4	96.2
	GaitGL[20]	96.0	98.3	99.0	97.9	96.9	95.4	97.0	98.9	**99.3**	98.8	94.0	97.4
	3DLocal [14]	96.0	99.0	99.5	**98.9**	**97.1**	94.2	96.3	**99.0**	98.8	98.5	95.2	97.5
	CSTL [13]	**97.2**	99.0	99.2	98.1	96.2	95.5	97.7	98.7	99.2	98.9	**96.5**	**97.8**
	GaitTransformer [7]	94.9	98.3	98.4	97.8	94.8	94.1	96.3	98.5	99.0	98.3	90.7	96.5
	GaitBase* [9]	-	-	-	-	-	-	-	-	-	-	-	97.6
	GaitGS (Ours)	97.1	**99.1**	99.1	98.1	96.5	**96.2**	**98.1**	98.7	99.0	**99.1**	94.5	**97.8**
BG	GaitSet [4]	86.7	94.2	95.7	93.4	88.9	85.5	89.0	91.7	94.5	95.9	83.3	90.8
	GaitPart [10]	89.1	94.8	96.7	95.1	88.3	84.9	89.0	93.5	96.1	93.8	85.8	91.5
	GaitGL [20]	92.6	**96.6**	96.8	95.5	**93.5**	**89.3**	92.2	**96.5**	**98.2**	96.9	91.5	**94.5**
	3DLocal [14]	92.9	95.9	**97.8**	**96.2**	93.0	87.8	**92.7**	96.3	97.9	**98.0**	88.5	94.3
	CSTL [13]	91.7	96.5	97.0	95.4	90.9	88.0	91.5	95.8	97.0	95.5	90.3	93.6
	GaitTransformer [7]	90.3	95.9	96.0	96.0	93.1	88.1	92.2	96.1	97.5	97.5	86.1	93.5
	GaitBase* [9]	-	-	-	-	-	-	-	-	-	-	-	94.0
	GaitGS (Ours)	**93.3**	96.5	96.4	94.8	92.8	89.0	91.9	96.2	97.8	97.1	**92.1**	94.4
CL	GaitSet [4]	59.5	75.0	78.3	74.6	71.4	71.3	70.8	74.1	74.6	69.4	54.1	70.3
	GaitPart [10]	70.7	85.5	86.9	83.3	77.1	72.5	76.9	82.2	83.8	80.2	66.5	78.7
	GaitGL [20]	76.6	90.0	90.3	87.1	84.5	79.0	84.1	87.0	87.3	84.4	69.5	83.6
	3DLocal [14]	78.2	90.2	92.0	87.1	83.0	76.8	83.1	86.6	86.8	84.1	70.9	83.7
	CSTL [13]	78.1	89.4	91.6	86.6	82.1	79.9	81.8	86.3	88.7	86.6	75.3	84.2
	GaitTransformer [7]	**81.5**	**91.9**	92.2	**91.2**	**85.9**	**83.1**	**86.8**	**90.7**	90.4	**89.0**	75.6	**87.1**
	GaitBase* [9]	-	-	-	-	-	-	-	-	-	-	-	77.4
	GaitGS (Ours)	80.7	90.2	**94.0**	90.2	85.6	81.9	85.5	89.3	**90.7**	87.6	**76.1**	86.5

4 Experiments

4.1 Datasets

CASIA-B. CASIA-B [34] is a popular dataset, which includes cross-view and multi-walking condition sequences of 124 subjects. Three walking conditions are considered: normal walking (NM, 6 groups), walking with bags (BG, 2 groups), and walking in coats (CL, 2 groups), with each group containing 11 different views. Moreover, we adopt Large-sample Training (LT) strategy, *i.e.*, subjects #001 ∼#074 are chosen as the train set and #075 ∼#124 as the test set.

GREW. GREW [38] is a large outdoor gait dataset with 128,671 sequences captured by 882 cameras from 26,345 subjects. GREW is typically divided into three parts, *i.e.*, training set (including 102,887 sequences from 20,000 subjects), validation set (including 1,784 sequences from 345 subjects), and test set (including 24000 sequences from 6000 subjects).

OU-MVLP. OU-MVLP [27] is a large dataset with cross-view sequences of 10307 subjects. It contains 2 groups denoted as Seq#00 and Seq#01, with each group including 14 different views. In our experiments, 5153 subjects are chosen as the train set, while the rest are the test set. During the test phase, Seq#00 and Seq#01 are taken as probe and gallery sequence respectively.

4.2 Implementation Details

Hyper-parameters. 1) For shallow feature extracting, the output channel is set to 32. For the CASIA-B dataset, Fine Branch Feature Extractor has three STEM blocks, with output channels set to 64, 64, and 128 for each block. In OUMVLP and GREW, an additional STEM block with output channel 256 is added. Additionally, the channel of the final output gait representation is set to 256. **2)** Horizontally pooling in MSFL divides the feature into 32 parts. **3)** The kernel size of the channel-grouped 1D convolution (K) for position encoding is set to 7. **4)** The head number of the self-attention block (N) is set to 8, and the number of the transformer layers (L) is set to 3 in CATM.

Training details. We adopt the Batch ALL (BA) sampling strategy in the training phase, where the batch size is set to $(8, 8)$ for CASIA-B, $(32, 8)$ for OU-MVLP, and $(32, 4)$ for GREW respectively.

The length and resolution of the gait sequence are set to 30 and 64×44. For all experiments, the margin m in Equation (13) is set to 0.25 and the weight α in Equation (12) is set to 0.2. Adam [15] is taken as the optimizer with the weight decay 5e-4, and the basic learning rate is set to 1e-4. Significantly, the learning rate of L-layer Transformer is set to $0.1\times$ as the other modules to ensure convergence of the loss. The number of iterations is set to 80k for CASIA-B, 210k for OU-MVLP, and 190k for GREW. The learning rate is reset to 1e-5 after 70k iterations for CASIA-B and after 150k iterations for OU-MVLP and GREW. For OU-MVLP, the learning rate is further reset to 1e-6 after 200k iterations. During testing, the entire sequence is fed into the network to extract gait representations.

4.3 Comparison with State-of-the-Art Methods

Evaluation on CASIA-B. As shown in Table 1, our method achieves Rank-1 accuracy of 97.8%, 94.4% and 86.5% on the NM, BG and CL conditions respectively. Compared to other methods, GaitGS performs best on NM condition, while it is 0.1% lower than GaitGL [20] on BG condition and 0.6% lower than GaitTransformer [7] on CL condition. However, as shown in Table 2, our method achieves the average Rank-1 accuracy of 92.9% for all conditions and outperforms other competitive methods such as GaitGL [20], 3DLocal [14], CSTL [13] and GaitTransformer [7] by 1.1%, 1.1%, 1.0% and 0.5% respectively. These results can be attributed to our method's enhanced ability to extract gait features and its powerful temporal modeling mechanism for granularity and span. In particular, GaitGS outperforms other methods on some parallel and vertical views due to its powerful temporal modeling ability and is less affected by the lack of spatial information.

Table 2: Comparison with GaitGL [20], 3DLocal [14], CSTL [13] and GaitTransformer [7] under the conditions of NM, BG and CL.

Methods	NM	BG	CL	Mean
GaitGL [20]	97.4	**94.5**	83.6	91.8
3DLocal [14]	97.5	94.3	83.7	91.8
CSTL [13]	**97.8**	93.6	84.2	91.9
GaitTransformer [7]	96.5	93.5	**87.1**	92.4
GaitGS (Ours)	97.8	94.4	86.5	**92.9**

Table 3: Rank-1 accuracy (%), Rank-5 accuracy (%), Rank-10 accuracy (%), and Rank-20 accuracy (%) on the GREW dataset.

Methods	Rank-1	Rank-5	Rank-10	Rank-20
GaitSet [4]	46.3	63.6	70.3	76.8
GaitPart [10]	44.0	60.7	67.3	73.5
GaitGL [20]	47.3	63.6	69.3	74.2
CSTL [13]	50.6	65.9	71.9	**76.9**
GaitGS (Ours)	**52.0**	**66.9**	**72.2**	76.6

Evaluation on GREW. GaitGS also performs very well on the outdoor dataset GREW. As shown in Table 3, our method achieves the hightest accuracy on Rank-1, Rank-5 and Rank-10. This indicates that our method has strong anti-interference ability in complex environments, and the generated gait representations are more discriminative and robust, making them more suitable for real-world scenarios.

Evaluation on OU-MVLP. We also evaluate our method on the largest public dataset OU-MVLP and compared it to other competitive methods. The results in Table 4 indicate that although our method performs second only to 3DLocal [14] on some views for OU-MVLP with invalid probe sequences, GaitGS achieves the highest Rank-1 average accuracy of 91.0%. Additionally, our method performs best on all views among some competitors and achieves the highest average Rank-1 accuracy of 97.5% for OU-MVLP without invalid probe sequences.

4.4 Ablation Study

We conduct several ablation experiments to demonstrate the effectiveness of key modules and parameter settings in our proposed method. The results are presented in the following tables, and we provide an analysis for each ablation experiment.

Effectiveness of granularity dimensional modeling. To verify the effectiveness of the fine and coarse branches, we conduct ablation studies by removing one of the two branches in both the MGFE and MSFL modules. Results from experiments shown in Table 5 demonstrate that both the fine and coarse branches are essential in GaitGS and help fully explore temporal information on different granularities. Notably, temporal aggregation operations like UTA may result in the loss of more gait information, so GaitGS without the coarse branch performs better than without the fine branch.

Effectiveness of span dimensional modeling. The results shown in Table 6 indicate that information from both global and local temporal spans is essential for temporal modeling and shows the

Table 4: Rank-1 accuracy (%) on OU-MVLP under 14 probe views excluding identical-view cases. The results of the first 8 rows and last 6 rows denote preserving and removing invalid probe sequences which have no corresponding labels in the gallery set, respectively.

Method	Probe View														Mean
	0°	15°	30°	45°	60°	75°	90°	180°	195°	210°	225°	240°	255°	270°	
GaitSet [4]	81.3	88.6	90.2	90.7	88.6	89.1	88.3	83.1	87.7	89.4	89.7	87.8	88.3	86.9	87.9
GaitPart [10]	82.6	88.9	90.8	91.0	89.7	89.9	89.5	85.2	88.1	90.0	90.1	89.0	89.1	88.2	88.7
GaitGL [20]	84.9	90.2	91.1	91.5	91.1	90.8	90.3	88.5	88.6	90.3	90.4	89.6	89.5	88.8	89.7
3DLocal [14]	86.1	91.2	**92.6**	**92.9**	**92.2**	91.3	91.1	86.9	**90.8**	92.2	92.3	**91.3**	**91.1**	**90.2**	90.9
CSTL [13]	87.1	91.0	91.5	91.8	90.6	90.8	90.6	89.4	90.2	90.5	90.7	89.8	90.0	89.4	90.2
GaitTransformer [7]	87.9	91.3	91.6	91.7	91.6	91.3	91.1	90.3	90.4	90.8	91.0	90.6	90.3	90.0	90.7
GaitBase [9]	-	-	-	-	-	-	-	-	-	-	-	-	-	-	90.8
GaitGS (Ours)	**88.4**	**91.6**	91.8	92.0	91.9	**91.5**	**91.2**	**90.7**	90.5	91.1	91.2	90.9	90.6	**90.2**	**91.0**
GaitSet [4]	84.5	93.3	96.7	96.6	93.5	95.3	94.2	87.0	92.5	96.0	96.0	93.0	94.3	92.7	93.3
GaitPart [10]	88.0	94.7	97.7	97.6	95.5	96.6	96.2	90.6	94.2	97.2	97.1	95.1	96.0	95.0	95.1
GaitGL [20]	90.5	96.1	98.0	98.1	97.0	97.6	97.1	94.2	94.9	97.4	97.4	95.7	96.5	95.7	96.2
3DLocal [14]	-	-	-	-	-	-	-	-	-	-	-	-	-	-	96.5
CSTL [13]	-	-	-	-	-	-	-	-	-	-	-	-	-	-	96.7
GaitGS (Ours)	**94.1**	**97.5**	**98.7**	**98.7**	**97.9**	**98.4**	**98.1**	**96.5**	**96.8**	**98.4**	**98.2**	**97.2**	**97.7**	**97.3**	**97.5**

progressiveness of our design. We can also observe that GaitGS without global temporal information performs much better than without local temporal information. The is because local information contains discriminative temporal and spatial features extracted by CNNs, which include short-term contextual clues in feature maps. Therefore, local temporal information is one of the most significant components for final gait representation and can seriously affect the performance of our method.

Table 5: Study of the effectiveness of the dual-branch design on the CASIA-B dataset.

Methods	NM	BG	CL	Mean
GaitGS *w/o* the coarse branch	97.5	93.1	84.3	91.6
GaitGS *w/o* the fine branch	97.5	93.0	82.8	91.1
GaitGS	**97.8**	**94.4**	**86.5**	**92.9**

Table 6: Study of the effectiveness of the CATM in MSFL on the CASIA-B dataset.

Methods	NM	BG	CL	Mean
GaitGS *w/o* global information	97.5	**94.4**	84.5	92.1
GaitGS *w/o* local information	92.8	81.8	66.6	80.4
GaitGS	**97.8**	**94.4**	**86.5**	**92.9**

Analysis of the kernel size of Position Encoding. The kernel size K of Position Encoding determines the range of adjacent frames for obtaining position information. The ablation experimental results are shown in Table 7. As the size of the kernel increases, the network performance improves initially and then decreases after $K = 7$. To ensure the accuracy of position embedding, we select the convolutional kernel of size 7.

Analysis of Transformer Layer. We investigate the impact of different layer settings L of transformer on network performance. The results shown in Table 8 indicate that as the number of transformer layers increases, network performance on CASIA-B initially improves and then decreases after $L = 3$. Therefore, we applied a 3-layer transformer in the CATM.

Table 7: Study of the kernel size (K) of Position Encoding on the CASIA-B dataset.

Kernel size	NM	BG	CL	Mean
$K = 3$	97.4	94.2	85.7	92.4
$K = 5$	97.7	**94.5**	**86.5**	**92.9**
$K = 7$	**97.8**	94.4	**86.5**	**92.9**
$K = 9$	97.6	94.3	85.6	92.5

Table 8: Study of the number (L) of the transformer layers in CATM on the CASIA-B dataset.

Method	NM	BG	CL	Mean
$L = 1$	97.5	**94.5**	86.2	92.7
$L = 2$	97.6	94.2	86.5	92.8
$L = 3$	**97.8**	94.4	**86.5**	**92.9**
$L = 4$	97.7	94.3	85.9	92.6

5 Conclusion

In this paper, we propose a novel gait recognition framework GaitGS, which effectively utilizes temporal information across diverse granularities and spans. The proposed MGFE comprises fine and coarse branches, enabling the capture of both micro-motion and macro-motion clues. Additionally, MSFL module generates position encoding adaptively, yielding comprehensive global and local

temporal gait representations. By aggregating temporal features with different granularities and spans, GaitGS produces more robust gait representations. Our extensive experimental results demonstrate the excellent performance of GaitGS. In the future, we plan to research lighter and more efficient temporal modeling methods in real-world scenarios. However, it is equally important to safeguard the privacy and security of individuals in everyday life settings. Adequate attention and measures should be taken to prevent potential privacy breaches through relevant regulations and policies. This will help to ensure that the use of gait recognition technology is both effective and ethical.

Acknowledgments

A Appendix

A.1 Comparison with other methods for input silhouettes with the size of 128×88

We conduct a comprehensive comparison between our method and other methods [4, 14, 12, 13] with input silhouettes of size 128×88 on the CASIA-B dataset. As shown in Table 9, our method achieves Rank-1 accuracy of 97.9%, 95.8% and 89.2% on the NM, BG and CL conditions respectively, which outperforms other competitive methods, leading to an average Rank-1 accuracy of 94.3%. Compared to other methods, the proposed GaitGS exhibits exceptional performance on the BG and CL conditions. These results highlight the robustness and effectiveness of our method in handling silhouettes of varying resolutions. Especially, our method outperforms in challenging conditions with high environmental noise, such as the CL condition. This achievement indicates the advantages of our robust temporal modeling aspect in resisting the impact of environmental noise.

Table 9: Rank-1 accuracy (%) on CASIA-B with different conditions for input silhouettes with the size of 128×88.

Method	Results on CASIA-B				
	input size	NM	BG	CL	Mean
GaitSet [4]	128×88	95.6	91.5	75.3	87.5
GLN [12]	128×88	96.9	94.0	77.5	89.5
3DLocal [14]	128×88	**98.3**	95.5	84.5	92.8
CSTL [13]	128×88	98.0	95.4	87.0	93.5
GaitGS (Ours)	128×88	97.9	**95.8**	**89.2**	**94.3**

A.2 Ablation Study on position encoding strategies in CATM

As shown in Table 10, our Channel-Adaptive Position Encoding strategy achieves the best performance on the CASIA-B dataset compared to alternative strategies, *i.e.*, no position encoding, sinusoidal position encoding [30] and 1D-Conv position encoding. The sinusoidal position encoding strategy provides preset fixed position information, which is hard to focus on the variability of different sequences. On the other hand, the 1D-Conv position encoding strategy makes the same position encoding across all channels, which disregards the distinct variability present in each channel. In contrast, our position encoding strategy employs grouped 1D-Conv, enabling the provision of more accurate and adaptive position information for transformers. This adaptability and accuracy contribute to its superior performance over the other strategies.

Table 10: Study of the different position encoding strategies in CATM on the CASIA-B dataset.

Position Encoding Strategy	NM	BG	CL	Mean
No position encoding	97.6	**94.4**	86.0	92.7
Sinusoidal position encoding [30]	97.6	94.2	86.1	92.7
1D-Conv position encoding	97.7	94.0	**86.5**	92.7
Ours	**97.8**	**94.4**	**86.5**	**92.9**

A.3 Visualization

In this section, we employ t-SNE [21] to visualize the feature distributions of our method. Figure 6 presents the visual comparisons between our method and other methods, *i.e.*, GaitSet [4] and GaitPart [10]. By the visualizations, we observe that our method exhibits denser feature distributions for the same subjects compared to the other methods. Conversely, the feature distributions of different subjects are more scattered and distinguishable. This proves the effectiveness of our method, which can extract highly discriminative and distinguishable feature representations. Therefore, our method has significant advantages in gait recognition tasks.

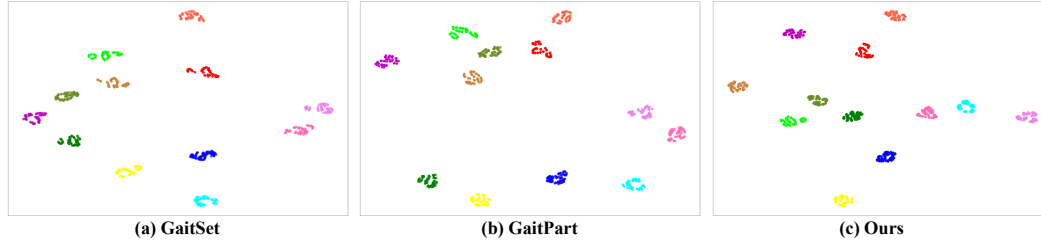**(a) GaitSet** **(b) GaitPart** **(c) Ours**

Figure 6: t-SNE visualization examples of our method and other methods for 12 selected subjects on the CASIA-B test dataset. The different colors represent distinct identities, allowing for easy distinguishment.

References

[1] An, W., Yu, S., Makihara, Y., Wu, X., Xu, C., Yu, Y., Liao, R., Yagi, Y.: Performance evaluation of model-based gait on multi-view very large population database with pose sequences. IEEE transactions on biometrics, behavior, and identity science **2**(4), 421–430 (2020)

[2] Balazia, M., Plataniotis, K.N.: Human gait recognition from motion capture data in signature poses. IET Biometrics **6**(2), 129–137 (2017)

[3] Cao, K., Jain, A.K.: Automated latent fingerprint recognition. IEEE transactions on pattern analysis and machine intelligence **41**(4), 788–800 (2018)

[4] Chao, H., Wang, K., He, Y., Zhang, J., Feng, J.: Gaitset: Cross-view gait recognition through utilizing gait as a deep set. IEEE Transactions on Pattern Analysis and Machine Intelligence pp. 1–1 (2021). https://doi.org/10.1109/TPAMI.2021.3057879

[5] Connor, P., Ross, A.: Biometric recognition by gait: A survey of modalities and features. Computer vision and image understanding **167**, 1–27 (2018)

[6] Cortes, C., Lawarence, N., Lee, D., Sugiyama, M., Garnett, R.: Advances in neural information processing systems 28. In: Proceedings of thGaitGe 29th Annual Conference on Neural Information Processing Systems (2015)

[7] Cui, Y., Kang, Y.: Gaittransformer: Multiple-temporal-scale transformer for cross-view gait recognition. In: 2022 IEEE International Conference on Multimedia and Expo (ICME). pp. 1–6 (2022). https://doi.org/10.1109/ICME52920.2022.9859928

[8] Dosovitskiy, A., Beyer, L., Kolesnikov, A., Weissenborn, D., Zhai, X., Unterthiner, T., Dehghani, M., Minderer, M., Heigold, G., Gelly, S., Uszkoreit, J., Houlsby, N.: An image is worth 16x16 words: Transformers for image recognition at scale. ICLR (2021)

[9] Fan, C., Liang, J., Shen, C., Hou, S., Huang, Y., Yu, S.: Opengait: Revisiting gait recognition toward better practicality (2022)

[10] Fan, C., Peng, Y., Cao, C., Liu, X., Hou, S., Chi, J., Huang, Y., Li, Q., He, Z.: Gaitpart: Temporal part-based model for gait recognition. In: Proceedings of the IEEE/CVF conference on computer vision and pattern recognition. pp. 14225–14233 (2020)

[11] Han, J., Bhanu, B.: Individual recognition using gait energy image. IEEE transactions on pattern analysis and machine intelligence **28**(2), 316–322 (2005)

[12] Hou, S., Cao, C., Liu, X., Huang, Y.: Gait lateral network: Learning discriminative and compact representations for gait recognition. In: Computer Vision–ECCV 2020: 16th European Conference, Glasgow, UK, August 23–28, 2020, Proceedings, Part IX. pp. 382–398. Springer (2020)

[13] Huang, X., Zhu, D., Wang, H., Wang, X., Yang, B., He, B., Liu, W., Feng, B.: Context-sensitive temporal feature learning for gait recognition. In: Proceedings of the IEEE/CVF International Conference on Computer Vision (ICCV). pp. 12909–12918 (October 2021)

[14] Huang, Z., Xue, D., Shen, X., Tian, X., Li, H., Huang, J., Hua, X.S.: 3d local convolutional neural networks for gait recognition. In: Proceedings of the IEEE/CVF International Conference on Computer Vision. pp. 14920–14929 (2021)

[15] Kingma, D.P., Ba, J.: Adam: A method for stochastic optimization. CoRR **abs/1412.6980** (2014)

[16] Lee, L., Grimson, W.E.L.: Gait analysis for recognition and classification. In: Proceedings of Fifth IEEE International Conference on Automatic Face Gesture Recognition. pp. 155–162. IEEE (2002)

[17] Li, G., Guo, L., Zhang, R., Qian, J., Gao, S.: Transgait: Multimodal-based gait recognition with set transformer. Applied Intelligence **53**(2), 1535–1547 (2023)

[18] Liao, R., Yu, S., An, W., Huang, Y.: A model-based gait recognition method with body pose and human prior knowledge. Pattern Recognition **98**, 107069 (2020)

[19] Lin, B., Zhang, S., Bao, F.: Gait recognition with multiple-temporal-scale 3d convolutional neural network. In: Proceedings of the 28th ACM international conference on multimedia. pp. 3054–3062 (2020)

[20] Lin, B., Zhang, S., Yu, X.: Gait recognition via effective global-local feature representation and local temporal aggregation. In: Proceedings of the IEEE/CVF International Conference on Computer Vision. pp. 14648–14656 (2021)

[21] Van der Maaten, L., Hinton, G.: Visualizing data using t-sne. Journal of machine learning research **9**(11) (2008)

[22] Nguyen, K., Fookes, C., Jillela, R., Sridharan, S., Ross, A.: Long range iris recognition: A survey. Pattern Recognition **72**, 123–143 (2017)

[23] Pinyoanuntapong, E., Ali, A., Wang, P., Lee, M., Chen, C.: Gaitmixer: skeleton-based gait representation learning via wide-spectrum multi-axial mixer. arXiv preprint arXiv:2210.15491 (2022)

[24] Sepas-Moghaddam, A., Etemad, A.: Deep gait recognition: A survey. IEEE transactions on pattern analysis and machine intelligence **45**(1), 264–284 (2022)

[25] Shen, C., Yu, S., Wang, J., Huang, G.Q., Wang, L.: A comprehensive survey on deep gait recognition: algorithms, datasets and challenges. arXiv preprint arXiv:2206.13732 (2022)

[26] Singh, J.P., Jain, S., Arora, S., Singh, U.P.: Vision-based gait recognition: A survey. Ieee Access **6**, 70497–70527 (2018)

[27] Takemura, N., Makihara, Y., Muramatsu, D., Echigo, T., Yagi, Y.: Multi-view large population gait dataset and its performance evaluation for cross-view gait recognition. IPSJ transactions on Computer Vision and Applications **10**, 1–14 (2018)

[28] Teepe, T., Gilg, J., Herzog, F., Hörmann, S., Rigoll, G.: Towards a deeper understanding of skeleton-based gait recognition. In: Proceedings of the IEEE/CVF Conference on Computer Vision and Pattern Recognition. pp. 1569–1577 (2022)

[29] Teepe, T., Khan, A., Gilg, J., Herzog, F., Hörmann, S., Rigoll, G.: GaitGraph: Graph convolutional network for skeleton-based gait recognition. In: 2021 IEEE International Conference on Image Processing (ICIP). pp. 2314–2318 (2021). https://doi.org/10.1109/ICIP42928.2021.9506717

[30] Vaswani, A., Shazeer, N., Parmar, N., Uszkoreit, J., Jones, L., Gomez, A.N., Kaiser, Ł., Polosukhin, I.: Attention is all you need. Advances in neural information processing systems **30** (2017)

[31] Wagg, D.K., Nixon, M.S.: On automated model-based extraction and analysis of gait. In: Sixth IEEE International Conference on Automatic Face and Gesture Recognition, 2004. Proceedings. pp. 11–16. IEEE (2004)

[32] Wang, C., Zhang, J., Wang, L., Pu, J., Yuan, X.: Human identification using temporal information preserving gait template. IEEE transactions on pattern analysis and machine intelligence **34**(11), 2164–2176 (2011)

[33] Yan, C., Zhang, B., Coenen, F.: Multi-attributes gait identification by convolutional neural networks. In: 2015 8th international congress on image and signal processing (CISP). pp. 642–647. IEEE (2015)

[34] Yu, S., Tan, D., Tan, T.: A framework for evaluating the effect of view angle, clothing and carrying condition on gait recognition. In: 18th international conference on pattern recognition (ICPR'06). vol. 4, pp. 441–444. IEEE (2006)

[35] Zhang, C., Chen, X.P., Han, G.Q., Liu, X.J.: Spatial transformer network on skeleton-based gait recognition. arXiv preprint arXiv:2204.03873 (2022)

[36] Zhang, Y., Huang, Y., Yu, S., Wang, L.: Cross-view gait recognition by discriminative feature learning. IEEE Transactions on Image Processing **29**, 1001–1015 (2019)

[37] Zhang, Z., Tran, L., Yin, X., Atoum, Y., Liu, X., Wan, J., Wang, N.: Gait recognition via disentangled representation learning. In: Proceedings of the IEEE/CVF Conference on Computer Vision and Pattern Recognition. pp. 4710–4719 (2019)

[38] Zhu, Z., Guo, X., Yang, T., Huang, J., Deng, J., Huang, G., Du, D., Lu, J., Zhou, J.: Gait recognition in the wild: A benchmark. In: Proceedings of the IEEE/CVF international conference on computer vision. pp. 14789–14799 (2021)